Small Scale HVDC Circuit Breaker

Originally published in:
IEEE Transactions on Components, Packaging and Manufacturing Technology 7(7), https://doi.org/10.1109/TCPMT.2017.2694058

Small Scale HVDC Circuit Breaker

Julien Thomas, Geraint Chaffey, *Student Member, IEEE,* and Christian M. Franck, *Senior Member, IEEE*

***Abstract*—Circuit breakers are anticipated for fault isolation in multiterminal HVDC networks, however, there are remaining challenges concerning the circuit breaker topology and operation. The passive oscillation principle circuit breaker is one of the topologies under consideration, the design of which requires examination of the arc characteristics. The design process is therefore presented, with the aim of constructing a small scale prototype. Firstly, a horizontal nozzle constricted arc setup with a blowing capability is built in order to study the stationary and transient arc characteristics $P(g)$ and $\tau(g)$, which are essential for the design of this type of breaker. Secondly, after their extraction from measurements, these two arc parameters are inserted into a simulation model based on the Mayr-Schwarz arc equation, which predicts an effective breaker operation. Finally, a passive oscillation principle breaker is constructed and successfully tested with both an arbitrary current source and on a scaled voltage source converter network.**

***Keywords*—arc interruption, HVDC circuit breakers, passive resonance, passive oscillation principle.**

I. Aim of the Study

HVDC circuit breakers are considered to be one of the key enabling technologies for future HVDC supergrids [1]–[4]. Substantial interest and research effort is thus currently invested into finding fast, reliable and efficient concepts for HVDC circuit breakers [5], with recent publication of several high power prototypes, for example [6], [7] and [8]. Several multiterminal systems have been developed, first implementing line commutated converters [9], [10], and recently with voltage source converters [11], [12], and although there are plans for system implementation of HVDC circuit breakers [13], little operational experience was gained. Requirement specifications and expected breaker-network interactions remain at a theoretical level.

At Imperial College London, a DC network is used for evaluation of mutual interaction of converter control concepts, including switching and fault clearing operations. The network emulates some characteristics of an HVDC system, consisting of a cable representation and two-level voltage source converters, which require protection against DC-side faults. For this purpose, a down-scaled HVDC circuit breaker is developed. The key challenge here is not to build any DC breaker able to clear a fault for the voltage source network specifications, but to build a circuit breaker using a technology also under discussion for HVDC networks. Using small scale models in this field is typically conducted to examine effects that cannot or are not simulated, and to provide verification of the simulated operation and control of a system.

Terminology within this paper is according to that defined in [14]. The time period between fault inception and the peak fault current is termed the fault neutralization time.

This manuscript is an extended and updated version of the prize winning paper *"Small scale HVDC circuit breaker"* submitted to the 2015 IEEE PES Student Prize Paper Award in Honor of T. Burke Hayes. Experimental work in Sections V to VI was conducted at ETH Zurich, whilst Section VI-B was conducted at Imperial College London.

II. Voltage Source Converter Network

To estimate the required fault neutralization time, the expected fault conditions on the voltage source network are first examined. The cable model is a pi-section representation, consisting of $22 \times 10\,\mathrm{km}$ sections (each $30\,\mathrm{m\Omega}$, $5\,\mathrm{mH}$, $3.6\,\mu\mathrm{F}$). The two-level converters are each $10\,\mathrm{kVA}$, each with a DC-side capacitance of $680\,\mu\mathrm{F}$ at a nominal voltage of $750\,\mathrm{V}$.

The nominal converter current is $10\,\mathrm{A}$, and the maximum acceptable current is $30\,\mathrm{A}$. The discharge of the converter's DC-side capacitance results in a very high rate of rise of fault current for a terminal fault case. The aim here is to evaluate the performance of the circuit breaker on a voltage source network, rather than specify a device that works under all scenarios. An additional inductance could be added, however in this case a mid-cable fault is chosen. For faults some distance along the cable, the fault current is also limited by the cable inductance; simplistic calculation suggests that a fault $50\,\mathrm{km}$ (5 pi-sections) from the converter would result in a fault current increasing at $30\,\mathrm{A/ms}$. Simulation study suggests that for a mid-line fault, travelling wave effects lead to a reduction in the average rate of change of current, resulting in a $30\,\mathrm{A}$ fault current after 4 ms, with an average rate of rise of $5\,\mathrm{A/ms}$.

The main breaker design constraint, imposed by the voltage source network, is the low fault neutralization time, being simulated to 4 ms.

III. HVDC Circuit Breaker Technologies

Breaker technologies proposed for HVDC applications can be classified into four circuit breaker categories; passive oscillation, active current injection, power electronic, or mechanical and power electronic hybrid [14]. The passive oscillation and active current injection circuit breakers operate with negligible losses but have large fault neutralization times. The electronic circuit breaker has a low fault neutralization time with a penalty of high losses, whilst the mechanical and power electronic hybrid circuit breaker has low losses, however both are expected to have high installation costs.

For each circuit breaker topology there are varying drawbacks and advantages regarding their fault neutralization times, their on-state losses, their peak fault current interruption capability and the economic cost of their components [15], [16].

The topology chosen for implementation on a future network depends on factors such as the protection system design and the network and converter topologies [17], therefore the requirements of circuit breakers in future HVDC networks are still under consideration.

IV. Development of an Arc Based Breaker

A fault neutralization time of 4 ms would normally reject the slower breaker technologies - contact separation with standard spring drives typically requires about 20 ms for topologies implementing mechanical elements. In the voltage source network under test, however, the fault is to be triggered by the grid operator. In the case of the passive oscillation principle circuit breaker, this gives the possibility to pre-open the contacts before the fault triggering, which drastically reduces the effective interruption time of these breakers given that the time required for contact separation is no longer accounted in the fault neutralization time. The contact motion speed in this case is therefore not a design boundary for this study. Hence the decision was taken to build a passive oscillation principle circuit breaker. Also, whilst this pre-opening would not be possible in a full-scale system, it allows for an examination of the oscillation and arc characteristics. However, if the contacts can be pre-opened, allowing the breaker to be in interruption position when the fault is triggered, it is absolutely necessary that the nominal current is not interrupted before.

The requirement for fast opening is effectively replaced with the requirement to selectively disable the excitation of resonance in the circuit breaker during nominal current and activate it after fault triggering. In order to fulfil this requirement, a nozzle constricted arc setup was built for arc characterization in different configurations (without/with blow and with different nozzle shapes) to decide on the resonance activation method. Arc characteristics were derived to simulate the breaker performance in a Simulink model, leading to an optimized breaker design. After the breaker construction, an optimal resonance activation strategy was experimentally investigated among several possibilities using a current source as a feeder: without/with blow at contact separation, partial or full contact separation with different nozzle shapes. Finally, the breaker was tested in the voltage source converter network.
Whilst the design of the interruption chamber for HVDC application cannot be transferred directly and follows different optimization goals, the entire design process as described can be directly applied and followed.

V. Passive Oscillation Circuit Breaker Design

A. Theoretical background

1) Passive oscillation circuit breakers: A passive oscillation circuit breaker (Fig. 1) is composed of three parallel branches: an AC breaker with an arc chamber in the main path, an LC commutation path for arc resonance excitation and an energy absorption path. This type of breaker passively excites a current oscillation between the LC commutation path and the switching arc, which may create an artificial current zero crossing in the main path breaker, at which arc extinction can occur if the arc cooling is sufficient.

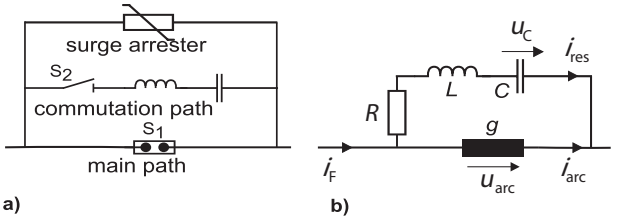

Fig. 1. Passive oscillation breaker; a) schematic, b) electrical equivalent circuit [15]

The artificial current zero crossing creation presupposes that the arc in parallel to the LC commutation path becomes unstable and causes a growing current oscillation i_{res}. This happens when:

$$\frac{\mathrm{d}u_{\mathrm{arc}}}{\mathrm{d}i_{\mathrm{arc}}} < -R\,. \tag{1}$$

This requires a gradient $\mathrm{d}u_{\mathrm{arc}}/\mathrm{d}i_{\mathrm{arc}}$ of the arc characteristic u_{arc} vs i_{arc}, negative (referred in the following as "negative characteristic") and larger than the positive parasitic resistance R of the commutation path [18]. From the preceding explanations, we can note that the knowledge of the UI arc characteristics is essential to use the principle of passive oscillation. It is therefore necessary to have a detailed arc model, which will be presented in Section V-A2.

A typical interruption process of a passive oscillation circuit breaker ($L = 130$ µH, $C = 28$ µF) has been modelled in Simulink [15] and is shown in Fig. 2. A 4 kA (steady-state) fault current interruption process is discussed. The current interruption process can be divided into the following steps:

i **Main contact S1 opening (here at t = 1 ms)**
An arc is drawn between the contacts at their separation. The arc is axially blown by the compression of a puffer volume physically coupled with the opening contact mechanism. Contact separation requires several milliseconds. The arc voltage rises approximately linearly with increasing distance of the contact opening (not modelled here) and stabilizes itself at full constant distance opening to a constant voltage (here 2 kV).

ii **Switch S2 of the commutation path closing**
When the switch S2 closes, the capacitor C is uncharged, while the arc voltage is at 2 kV. This voltage difference causes an inrush current into the capacitor and excites a current oscillation between the arc and the LC commutation circuit, here of $i_{\mathrm{res}} \approx$ 1.3 kA.

iii **Passive resonance**
The arc and the LC commutation path form an unstable resonance circuit. Oscillating currents i_{arc} and

i_{res} increase in amplitude.

iv **Arc extinction**
When the oscillation amplitude of the commutation path i_{res} becomes larger than the fault current i_F, a current zero crossing of the arc current i_{arc} in the main path is created (here at 6.5 ms). If the forced cooling is sufficient, arc extinction occurs at this zero crossing. At extinction, the full fault current commutates to the resonance path ($i_{res} = i_F$).

v **Capacitor charging**
The resonance capacitor is charged to the breakthrough voltage of the surge arrester (here at 210 kV).

vi **Voltage limitation**
Once the capacitor voltage exceeds the breakthrough voltage of the surge arrester, the fault current commutates from the resonance path to the surge arrester path (here at t = 8 ms).

vii **Energy absorption**
The remaining inductive energy stored in the network is absorbed by the surge arrester, which forces the fault current i_F to decrease to zero.

2) Arc modelling: Due to their low calculation effort and reasonable accuracy, black-box models are widely used to simulate dynamic arc-network interactions. They have been successfully applied to describe free burning as well as nozzle constricted arcs and are therefore used to predict passive oscillation arc behaviour [15].

The selected arc modelling is based on the the Mayr-equation [19] and can be formulated as:

$$\dot{g} = \frac{\mathrm{d}g}{\mathrm{d}t} = \frac{1}{\tau}\left(\frac{i_{arc}^2}{P_{cool}} - g\right) . \tag{2}$$

τ is the thermal inertia and can physically be interpreted as the characteristic time with which the arc would exponentially approach its new steady-state after a sudden change in P_{cool} or i_{arc} [20].

Data revealed that the cooling power P_{cool} and the thermal inertia τ were not constant but functions of different physical parameters. This is why Schwarz applied a functional dependency of P_{cool} and τ of the conductance g for re-computation of switching arcs [22]. Schwarz introduced the so called generalized Mayr's equation or Mayr-Schwarz arc equation where *P(g)* and *τ(g)* are free functions of the arc conductance g:

$$\dot{g} = \frac{g}{\tau(g)}\left(\frac{u_{arc} i_{arc}}{P(g)} - 1\right) . \tag{3}$$

Also, the assumption of power law dependency introduced by Pietsch [23], describing the arc behaviour with higher precision than with constant arc parameters, was adopted for the arc modelling:

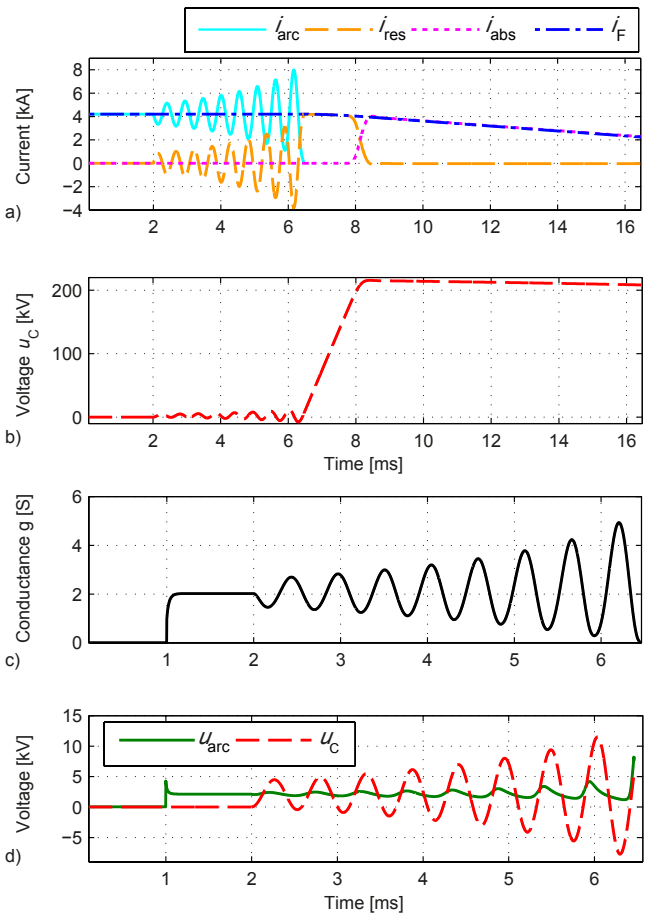

Fig. 2. Passive oscillation current interruption [15]: a) fault current (i_F) commutation from the main path (i_{arc}) to the resonance path (i_{res}) and further to the energy absorber path (i_{abs}), b) capacitor C charging, c) arc conductance (g) oscillation zoom, d) Arc voltage (u_{arc}) and capacitor voltage (u_C) oscillation zoom

$$P(g) = a \cdot g^b , \tag{4}$$

$$\tau(g) = c \cdot g^d . \tag{5}$$

These commonly used approximations of arc characteristics correctly describe certain types of arcs in a limited conductance range but are often used for characterization of switching arc chambers [15]. Experimental results have indicated that passive resonance is very sensitive to the arc parameters $P(g)$ and $\tau(g)$, therefore a very precise knowledge of these two potential functions is central to assess if the excitation of arc instability, and therefore arc extinction using passive resonance, is possible for a selected arc arrangement.

B. Arc characterization

1) Arbitrary current source: A current source allowing testing with nearly arbitrary current waveforms, including steps

and slopes of varying steepness, was used for precise stationary and dynamic arc characterization [20], [21]. It consists of three parallel interleaved modules with a capability to provide a voltage of 3 kV and a current of 1 kA each and is equipped with a common controller. The load current i_{load} is the superposition of all three module currents i_n. The working principle of the current source (Fig. 3) is similar to the one of a buck converter [24].

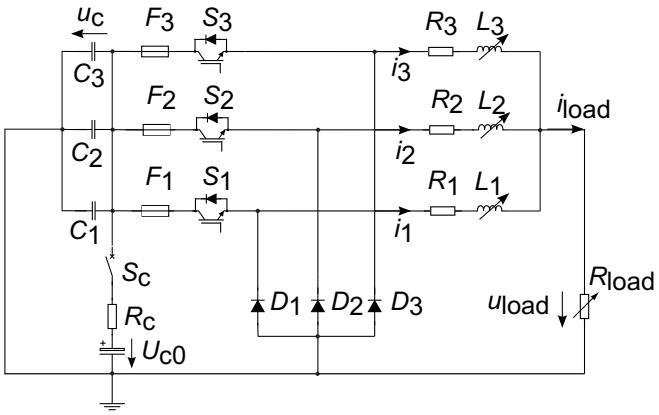

Fig. 3. Electrical equivalent circuit of the arbitrary current source [24]

2) Method of $P(g)$ and $\tau(g)$ determination: Based on the ability of the current source to create nearly arbitrary waveforms, a method was developed to determine the arc parameters $P(g)$ and $\tau(g)$ as free functions of the arc conductance g. This method uses the generalized Mayr's equation (3) for arc modelling and consists of the creation of a combination of fast current spikes and constant current plateaus. The constant plateaus are used to determine the stationary arc characteristics, whereas fast current spikes are used to determine the transient arc characteristics. A suitable current waveform and its corresponding voltage is shown in Fig. 4.

The specific determination algorithm is detailed below:

i A current waveform is shaped to have constant amplitude plateaus for a time $t > 5\tau$ to ensure establishment of quasi stationary conditions. The thermal inertia τ is experimentally known to be in the range of 20µs. During each plateau phase, several spikes of time duration τ are superimposed.

ii The averaged current and voltage of several k plateaus form k couples $[i_{\text{arc}};u_{\text{arc}}]$, from which a fitted UI characteristic can be deduced (Fig. 5). If necessary, for low currents, the last current decay and the corresponding voltages (see the green dotted circle in Fig. 4) can be used to get additional couples $[i_{\text{arc}};u_{\text{arc}}]$.

iii The stationary heating power $P_{\text{heat}}(g)$ follows directly as $P_{\text{heat}} = u_{\text{arc}} i_{\text{arc}}$ and $g = i_{\text{arc}}/u_{\text{arc}}$. This heating power can then be fitted to equation (4) (Fig. 6).

iv In order to find the arc thermal inertia $\tau(g)$, the fast current spikes superimposed on each plateau need to be separately analysed (Fig. 7).

v The transient heating power $P_{\text{heat}}(g)$, being described as for the stationary case, by $P_{\text{heat}} = u_{\text{arc}} i_{\text{arc}}$ and $g = i_{\text{arc}}/u_{\text{arc}}$, one stationary value $P_{\text{heat}_1}(g_1)$ is determined from the constant current time period as close as possible before the spike (see green dotted circle in Fig. 7).

vi The point of maximum conductance $g_{\max}$ being an extremum $\dot{g}_{\max} = 0$ and therefore a dynamically occurring stationary point according to Rijanto [25], the two stationary points $P_{\text{heat}_1}(g_1)$ and $P_{\text{heat}_{\max}}(g_{\max})$ are linearly interpolated (Fig. 8) using:

$$P_{\text{lin}} = x \cdot g + y \,, \tag{6}$$

with :

$$x = \frac{P_{\text{heat}_{\max}}(g_{\max}) - P_{\text{heat}_1}(g_1)}{g_{\max} - g_1} \,, \tag{7}$$

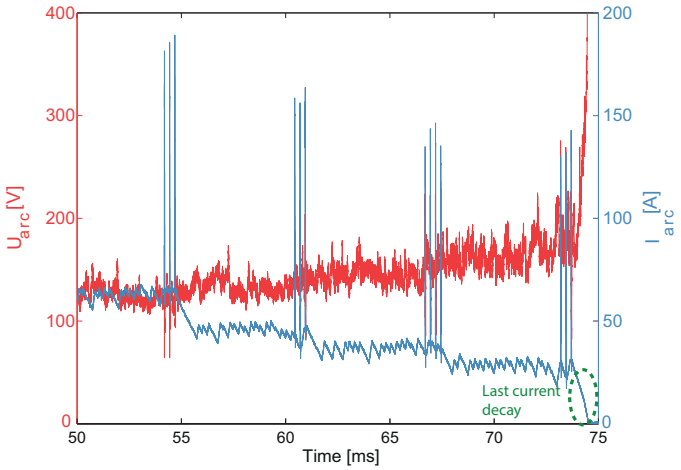

Fig. 4. Example of optimal current waveform and its corresponding voltage, for use of the detailed algorithm

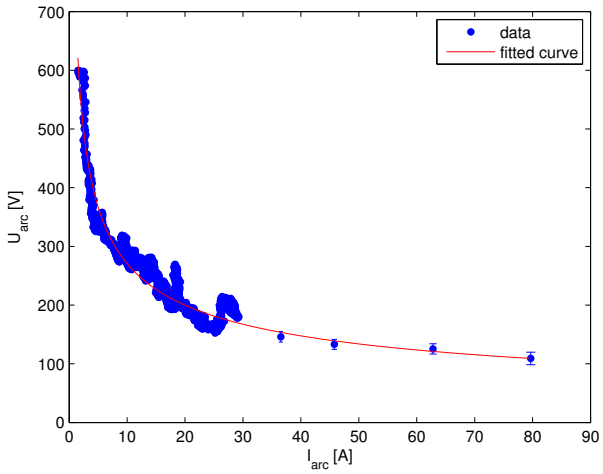

Fig. 5. (Negative) quasi stationary UI characteristic ($k = 3567$)

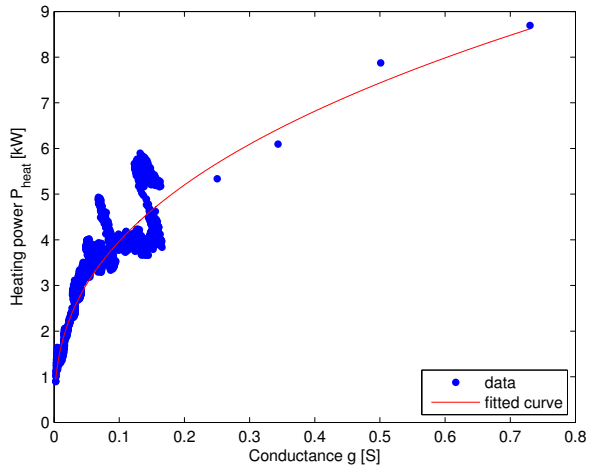

Fig. 6. Heating power P_{heat} vs conductance g
Fitting: $P(g) = 9.75\text{kW} \cdot g^{0.39}$

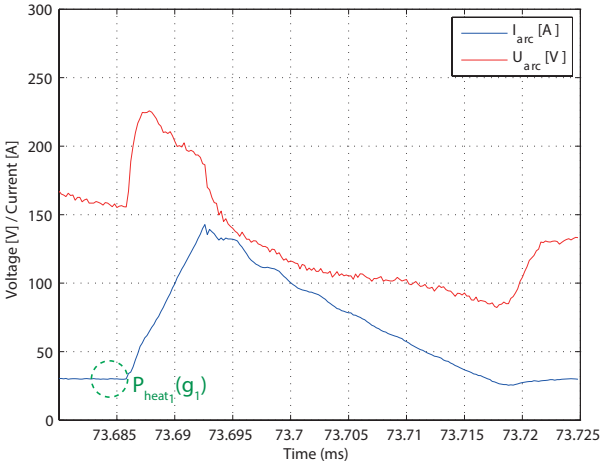

Fig. 7. Arc voltage response to a current spike

and :

$$y = P_{\text{heat}_1}(g_1) - x \cdot (g - g_1)\,. \tag{8}$$

vii The chosen model equation (here the Mayr-Schwarz arc equation (3)) is solved for the current gradient:

$$\dot{g}^* = \frac{1}{\tau}\left(\frac{i_{\text{arc}}^2}{P_{\text{lin}}} - g\right) \tag{9}$$

where g and i_{arc} are given by measurements, while P_{lin} comes from simulation using equation (6).

viii Iteratively, the least square error

$$\sum(\dot{g} - \dot{g}^*)^2 \tag{10}$$

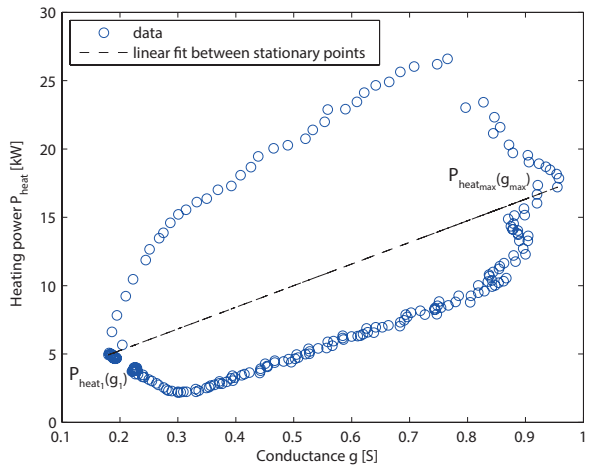

Fig. 8. Heating power P_{heat} vs conductance g of one current spike

is minimized by modifying τ with a start guess of $\tau = 10$ µs, where the conductance $\dot{g}$ has been smoothed and $\dot{g}^*$ obtained by simulation. This minimization, gives therefore one optimal couple $[g_{opt};\tau_{opt}]$, corresponding to one spike of one plateau. By repeating the operation for the m spikes of the n plateaus, several couples $[g_{opt_{mn}};\tau_{opt_{mn}}]$ can be found.

ix Finally, τ can be fitted as the desired thermal inertia potential function (equation (5)) or taken as a constant.

3) Nozzle constricted arc:

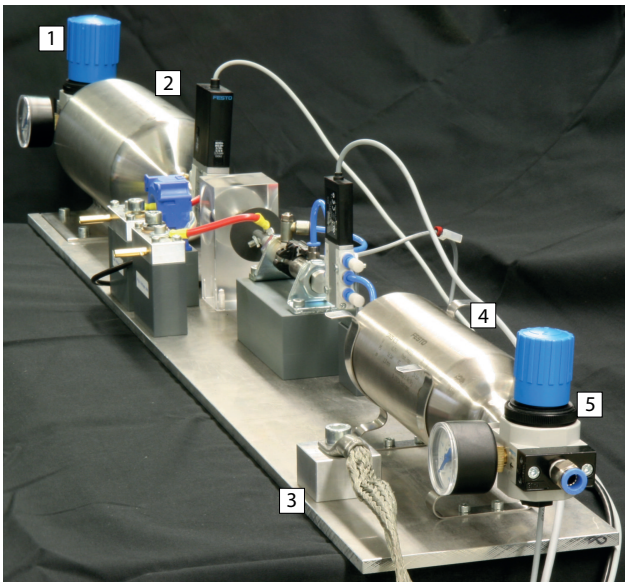

1 Blowing pressure regulator
2 Compressed air reservoir 2l
3 Ground connector
4 Compressed air reservoir 0.75l
5 Piston cylinder pressure regulator

Fig. 9. Nozzle constricted setup

a) Experimental setup: A nozzle constricted arc setup, with a blowing capability, was designed and manufactured (Fig. 9 and Fig. 10), as it has been shown that an axial blow of arc increases its negative characteristic [15]. The aim of this experimental setup was first to observe if the quasi stationary UI arc characteristic was negative, which is a prerequisite for passive oscillation arc excitation, in unblown as in blown conditions and secondly to derive the arc parameters $P(g)$ and $\tau(g)$.

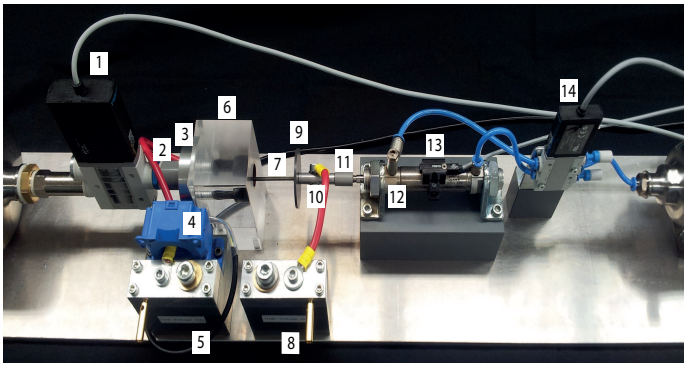

1 Blowing valve
2 Valve insulator
3 Fixed electrode
4 Current sensor
5 LV terminal
6 Nozzle
7 M3 threaded rod
8 HV terminal
9 Protection disk
10 Moving electrode
11 Cylinder insulator
12 Piston rod cylinder
13 Position transmitter
14 Cylinder valve

Fig. 10. Nozzle constricted setup components

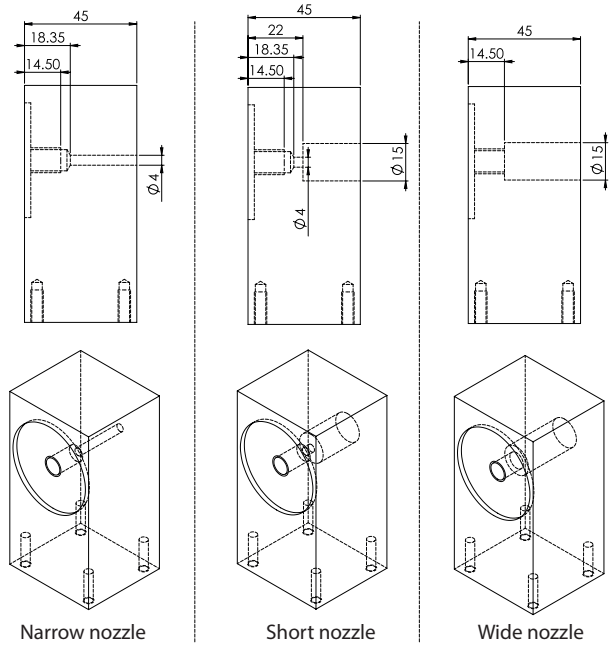

Fig. 11. Nozzles (dimensions in mm)

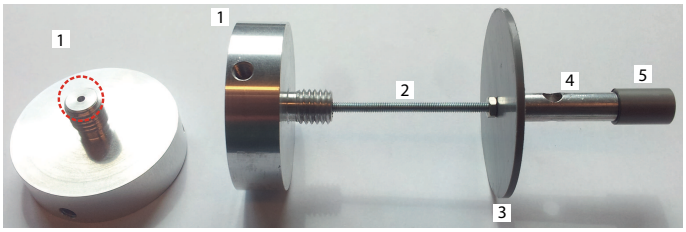

1 Fixed electrode
2 M3 threaded rod
3 Protection disk
4 Moving electrode
5 Cylinder insulator

Fig. 12. Contacts

The main components of this nozzle constricted arc setup are presented in the following:

- *Nozzles:* In order to study the decisive effect of the nozzle shape on the arc characteristics, three different nozzles (narrow nozzle, short nozzle, wide nozzle) shown in Fig. 11, were manufactured in PMMA (plexiglas). The idea behind the design shape of these three nozzles was to observe any difference in the arc characteristics, first when the nozzle walls constrict the arc (narrow nozzle), secondly when the arc is almost not constricted (wide nozzle) and finally when the nozzle arc chamber is a mix of both cases (short nozzle).

- *Contacts:* The low voltage electrical contact, called the fixed electrode, was made of aluminium. The high voltage electrical contact was composed by an M3 threaded rod made of steel, screwed to the so called moving electrode, made of aluminium. These electrical contacts are shown in closed position in Fig. 12. The 2 mm diameter hole drilled in the fixed electrode, where the compressed air flows to blow the arc after contact separation, is highlighted in a red dotted circle.

- *Contact movement:* A *Festo* cylinder DSNU-16-25-PPS-A with self-adjusting pneumatic end-position cushioning was used in combination with a 5/2 monostable fast-switching solenoid valve MHE2-MS1H-5/2-QS-4-K. The stroke of the piston is 25 mm. The full contact separation requires about 45 ms with 3 bar relative pressure.
- *Blowing system:* A *Festo* fast-switching solenoid valve MHE4-MS1H-3/2G-1/4-K was used to initiate the gas flow that blows the arc in the nozzle. The full opening switching-on time of this 3/2 normally closed monostable valve is 3.5 ms. Its nominal diameter is 4 mm.
- *Microcontroller:* In order to control the breaker, an *Arduino Due* microcontroller was used, because contact opening and blowing are physically uncoupled, unlike commercial puffer and self-blast breakers. The use of a microcontroller, particularly in combination with a contact position transmitter and its digital signal converter, allowed an automatic coupling and a precise scheduling of the blowing and the contact opening processes. The blowing can be started at any desired

moment during contact separation, by adjusting the location of the position transmitter along the piston rod cylinder. This offered the possibility to test different breaker control strategies presented in Section VI-A1 (without/with blowing at contact separation, at partial or at full contact opening).

b) Nozzle study: The influence of the nozzle shape on the arc characteristics (i.e. on the quasi stationary UI characteristic, on $P(g)$ and $\tau(g)$) at full contact opening in blown (2 bar) and unblown conditions, was assessed for the three nozzles. Additionally, by removing the nozzle of the nozzle constricted arc setup, the arc was studied in a horizontal free burning arc arrangement. The nozzle constricted setup was placed as load of the arbitrary current source (see Fig. 3) and thus $i_{\text{load}} = i_{\text{arc}}$. In total, this represented eight cases of which the fitted UI characteristics are plotted in Fig. 13.

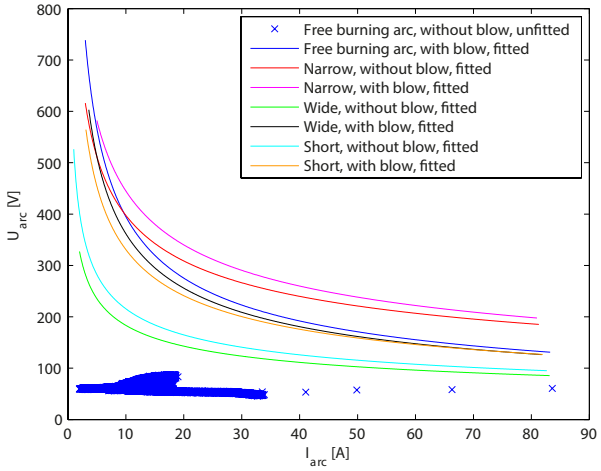

Fig. 13. Fitted UI characteristics comparing three different nozzles in unblown and blown conditions

The measurements clearly show that a negative UI characteristic is inherently available when a nozzle is used. This negative characteristic is present not only in the cases where a blow is used to boost the resonance excitation, but also in unblown conditions. To the contrary, the horizontal free burning arc arrangement does not show any negative characteristic, except if the arc is blown. For each of the four arrangements, the slope of the UI characteristic in the blown case is mostly steeper than the one in unblown conditions, which indicates that the blowing is expected to speed up the resonance and therefore the arc extinction. These measurements confirm the relevancy of the construction of a nozzle constricted setup, which is expected to boost passive resonance due to the observed falling slope of the quasi stationary UI characteristic, either by constriction of the arc with a nozzle or by the use of a blow or by a combination of both effects. Arc extinction using passive resonance is thus expected to be successful.

4) Design options for small scale circuit breaker: The expected breaker behaviour, based on the measured arc characteristics in Section V-B3b, was simulated with different combinations of inductances and capacitances for the resonant path. Main inputs to this breaker simulation code, written during the dissertation in [15], are the exponential functions $P(g)$ and $\tau(g)$, the inductor, as well as the capacitor and the parasitic resistance values of the commutation path. After the arc characteristics were determined in Section V-B3b, the values of the inductor and the capacitor needed to be chosen. The chosen method was to iteratively simulate the breaker behaviour with various commercially available capacitances and various self-made inductances. A suitable combination should lead to arc extinction in less than the 4 ms, as defined by the voltage source network requirements. The following reasonable values showed suitable simulation results (performed with an approximate $\tau(g) = 10\,\mu\text{s} \cdot g^{0.4}$ and $P(g) = 10\,\text{kW} \cdot g^{0.4}$) and components in their range should be used for the breaker:

- $L = 30$ µH ,
- $C = 50$ µF .

Fig. 14 shows the predicted creation of oscillations at an appropriate frequency (f_0 = 4.1 kHz), expected to meet the network interruption time requirements.

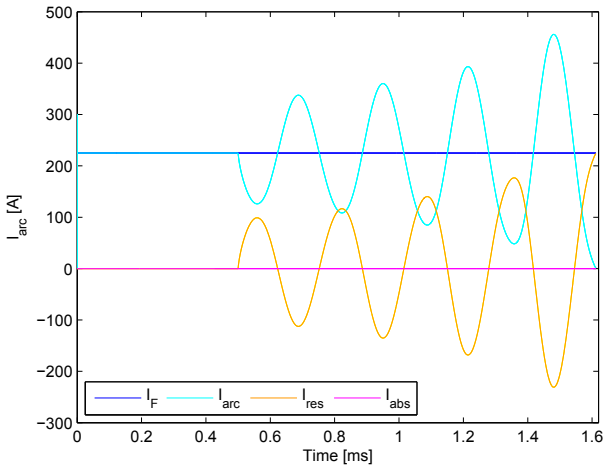

Fig. 14. Resonance simulation

C. Design of a passive oscillation small scale HVDC circuit breaker

The small scale passive oscillation circuit breaker designed (Fig. 15 and Fig. 16), is a size-optimized update of the nozzle constricted setup built and presented in Section V-B3a, where a LC resonance path for artificial current zero crossing creation and varistors for energy absorption have been added.

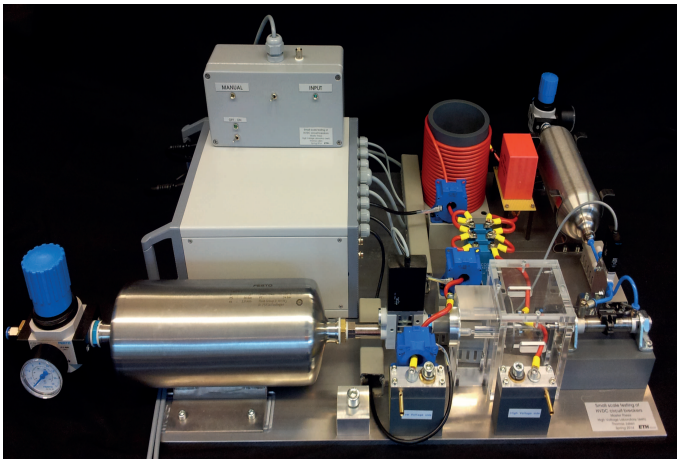

Fig. 15. Passive oscillation circuit breaker

The contact separation and the blowing process are achieved by the same components (pressure regulators, compressed air reservoirs, connectors,valves, insulators, electrodes, nozzles) as in the nozzle constricted setup. The main new added components are presented in the following.

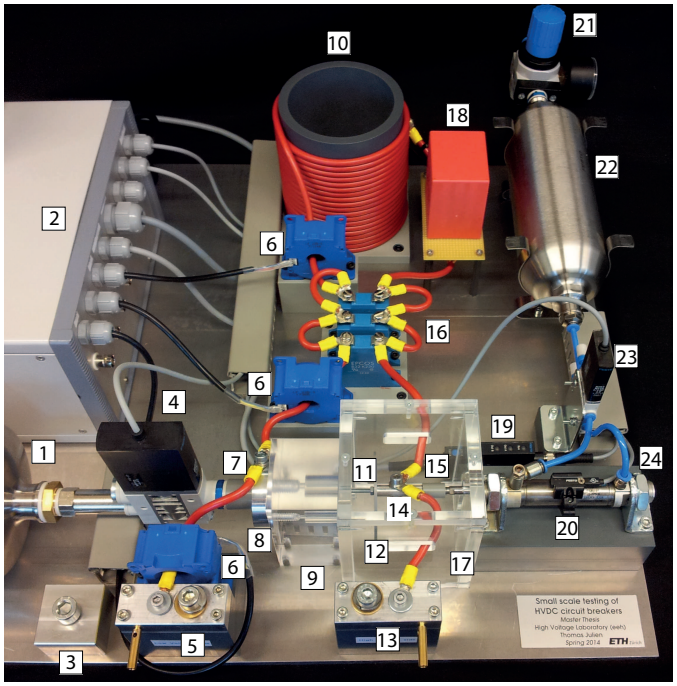

1 Compressed air reservoir 2l
2 Supply box
3 Ground connector
4 Blowing valve
5 LV terminal
6 Current sensors
7 Valve insulator
8 Fixed electrode
9 Nozzle
10 Inductor
11 M3 threaded rod
12 Protection disk
13 HV terminal
14 Moving electrode
15 Cylinder insulator
16 Varistors
17 Protection box
18 Capacitor 60uF
19 Signal converter
20 Position transmitter
21 Piston cylinder pressure regulator
22 Compressed air reservoir pressure regulator 0.75l
23 Cylinder valve
24 Piston rod cylinder

Fig. 16. Passive oscillation circuit breaker components

1) LC commutation path: The LC commutation path is composed by a 60 µF capacitor with a rated voltage of 1100 V and a 220 µH inductor in series (f_0 = 1.4 kHz).

2) Energy absorption path: Three *EPCOS* metal oxide varistors B32K230 in parallel are composing the breaker energy absorption path.

3) Current sensors: Three current sensors, CS_n, placed in the breaker (Fig. 17), allow the direct measurement or the deduction by subtraction of the currents flowing in every branch of the breaker.

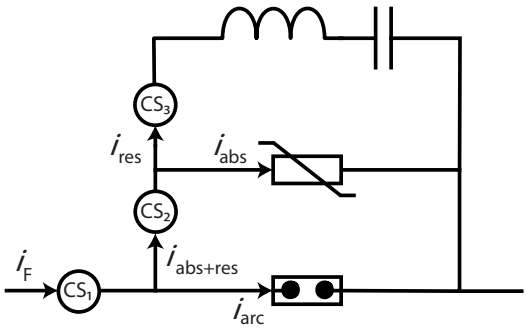

Fig. 17. Current sensor locations in the circuit breaker

VI. Circuit Breaker Operation

A. Breaker testing with the arbitrary current source

During a first testing phase, the breaker was placed as load of the arbitrary current source (see Fig. 3) and thus $i_{\text{load}} = i_{\text{F}}$. Due to the working principle of this current source, which provides a programmed current profile until its capacitors discharge, it should be noted that fault current decay to zero cannot be directly observed.

An experimental current interruption process is detailed in Fig. 18, including the different phases leading to arc extinction with a passive oscillation circuit breaker, as presented in Section V-A1. From 20 to 25 ms, growing current oscillations are passively excited in the main path (i_{arc}) as well as in the resonant path (i_{res}). The currents i_{arc} and i_{res} are in antiphase, because the equality $i_{\text{arc}} + i_{\text{res}} = i_{\text{F}}$ must hold, as stated by the Kirchhoff's current law.

At about 25 ms, i_{res} becomes larger than i_{F}, creating an artificial current zero crossing in the main path, which leads to arc extinction ($i_{\text{arc}} = 0$). At arc extinction, the full fault current commutates to the resonance path ($i_{\text{res}} = i_{\text{F}}$).

Between 25 and 26 ms, the capacitor of the commutation path is charged and limited to the breakthrough voltage of the varistors (about 475 V) situated in the energy absorption path.

From 25 to 28 ms, the fault current i_{F} commutates from the resonant path to the absorber path. At about 28 ms, the equality $i_{\text{abs}} = i_{\text{F}}$ holds and in a real network, the inductive energy would be dissipated and the current would decay to zero.

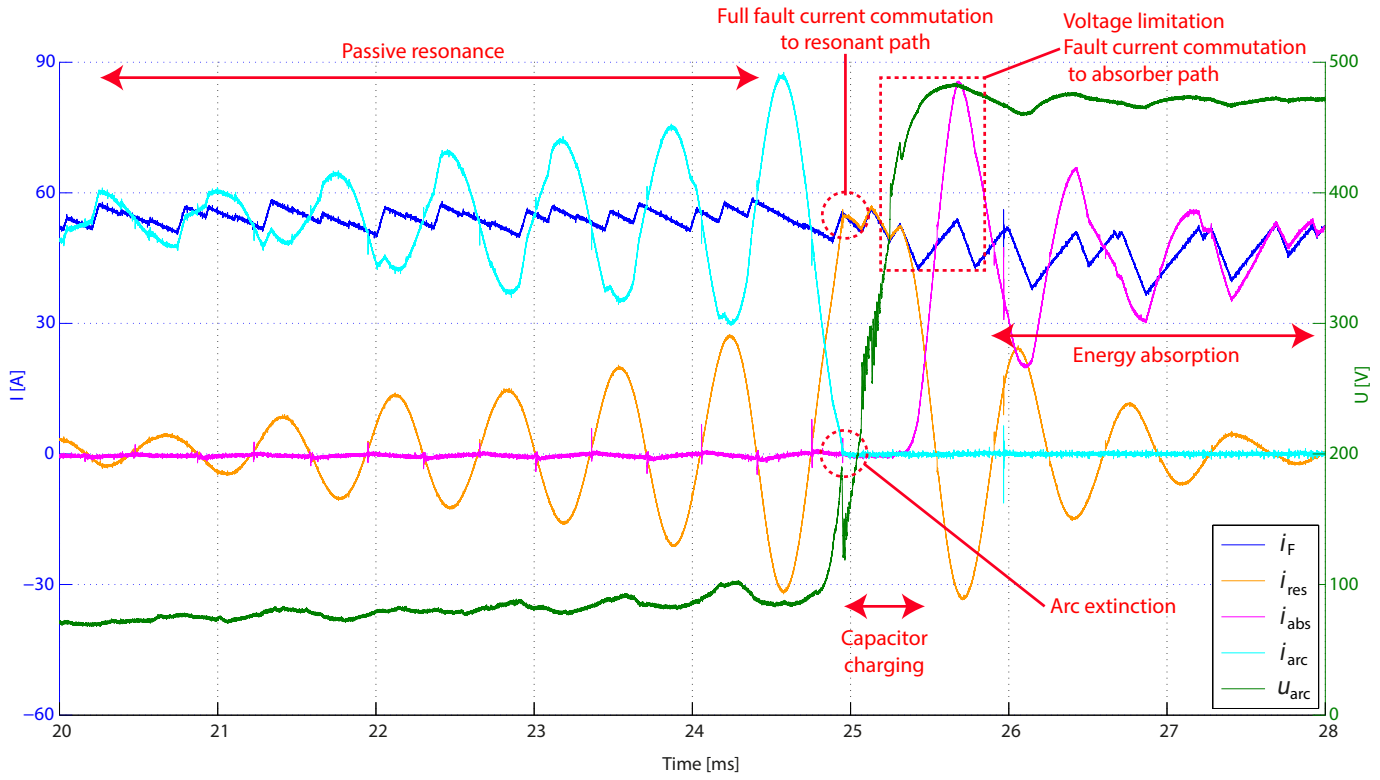

Fig. 18. Current interruption process, narrow nozzle, without blow, (f_0 = 1.4 kHz)

1) Strategies: Three different resonance excitation strategies in combination without/with one of the nozzles were studied with a fault current $i_F = 60$ A: no blow, blow at contact separation, blow at full contact separation. This represented a total of twelve cases. These measurements confirmed the conclusions of the nozzle study (Section V-B3b) - that passive resonance could be excited if the arc is constricted by a nozzle or if there is a blow or a combination of both effects. Furthermore, they confirmed for each of the four arrangements that blowing the arc is speeding up the resonance (at contact separation or at full contact separation), even if this effect could not be directly observed in the case of the narrow and short nozzles in the exact same measurement conditions as in the arc characterization of Section V-B3b, because the natural resonance in these two arrangements extinguished the arc before full contact separation. The three strategies are commented in the following for the narrow nozzle. The active current injection, occurring at contact separation and resulting from the difference of voltage between the arc voltage and the uncharged capacitor of the LC path, should be noted.

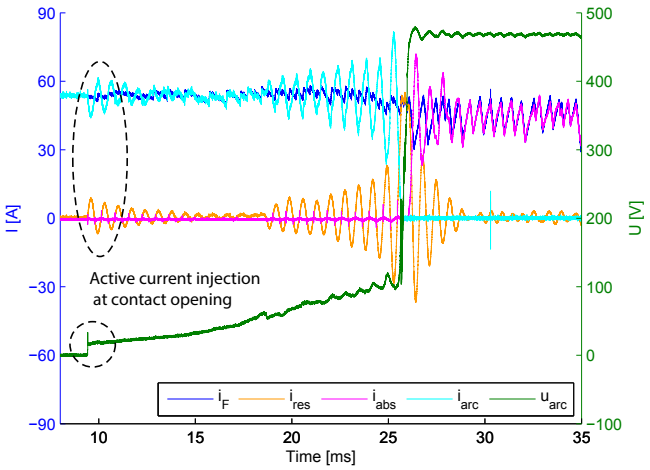

Fig. 19. Narrow nozzle, without blow

a) Without blow: The breaker without any blowing effect, leads to arc extinction after about 25 ms, i.e. 16 ms after contact separation. This strategy is too slow for implementation in the voltage source network under examination.

b) With blow at contact separation: The breaker with a blowing effect at contact separation, leads to arc extinction after about 13.5 ms, i.e. 4 ms after contact separation. This is

a feasible strategy for the voltage source network.

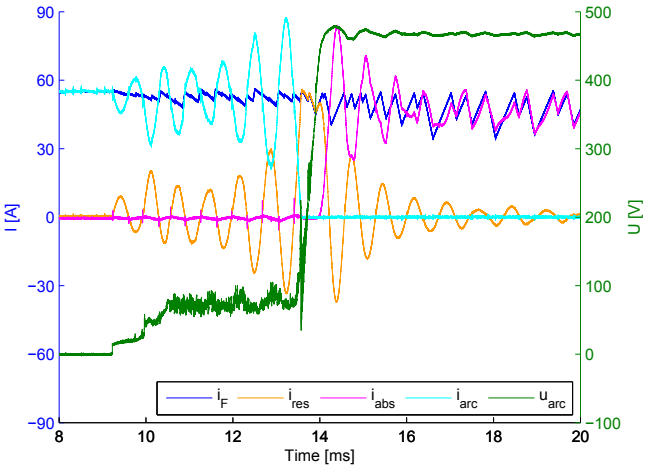

Fig. 20. Narrow nozzle, with blow at contact separation (2bar)

c) With blow at full contact separation: As the arc extinction already occurs without any blowing effect after about 25 ms, i.e. 16 ms after contact separation, the effect of the blow cannot be studied at full contact separation.

2) Optimal strategy - With blow at partial contact separation: A last blowing strategy at partial contact separation was studied, based on the measurements with the narrow nozzle without blow (Fig. 18 and Fig. 19) and is shown in Fig. 21. Fig. 18 shows a natural resonance starting at about 20 ms (i.e.

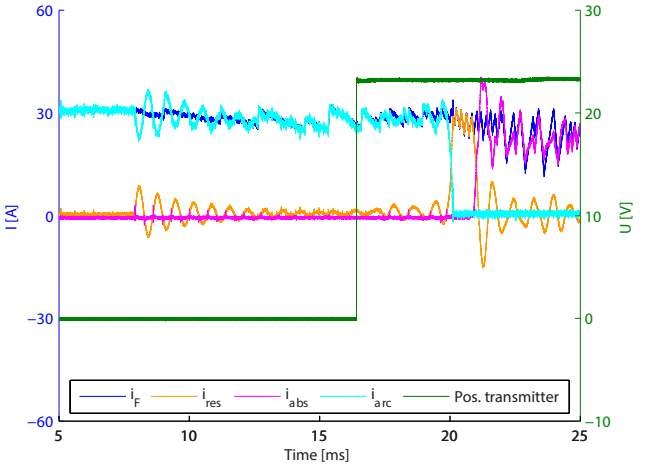

Fig. 21. Optimal strategy: Narrow nozzle, with blow at partial contact separation (2 bar)

the UI arc characteristic seems to be negative only from this time because growing oscillations are observable). The concept of this strategy is to start to blow at 20 ms, to take advantage of this natural resonance, and to speed up the growth of the current oscillations. The testing was made with $i_F = 30$ A and the 24 V position transmitter signal triggering the blowing valve is shown in green (effective blowing starts 3.5 ms after). This strategy shows the fastest and most repeatable resonance (less than 2 ms) and was used in the voltage source network.

B. Breaker testing in a VSC network

1) Network description: The voltage source network consists of two-level voltage source converters which inherently feed an uncontrolled current into a low impedance DC fault. Reliable implementation on a multiterminal network is therefore likely to require DC circuit breakers for fault protection. A cable is emulated using 44 pi-sections, in total representing 220 km of XLPE and exhibiting some of the transient properties of a cable that cannot be emulated with a simpler representation. The fault is generated using an IGBT and a resistor allowing for the synchronised timing of the fault inception and the circuit breaker operation.

2) Testing: The breaker-network interaction in the case of a fault occurring in the middle of a 100 km line (Fig. 22), was studied. Fault current was measured at location CS_1. In the absence of the passive oscillation breaker operation, the fault current profile would reach about 40 A, as shown in Fig. 23, in which the fault triggering occurs at 0 ms. At 40 A, the fault current is isolated by a semiconductor switch to prevent damage to the converter. The overcurrent is detected by the converter, which disables its IGBTs, and a fault current is conducted through the freewheeling diodes. Following the fault, the converter voltage remains at a magnitude determined by the natural rectification of the converter's AC-side voltage. The fault current profile correlates well with simulation results; it is observed that the initial fault current rises at a rate of 31 A/ms, however the travelling wave effects lead to an average rate of rise of 8.2 A/ms. The observed period of the disturbance, 1.4 ms, corresponds to the time for the fault wave to travel 100 km (50 km to the converter terminal and 50 km back to the circuit breaker), 1.34 ms.

Fig. 24 shows the operation of the circuit breaker following a fault mid-way along the cable. The arc was extinguished after about 11 ms after contact separation and about 1 ms after fault triggering (11 ms). Full fault clearance occurs 24 ms after contact opening.

VII. Conclusion and Outlook

Based on the essential process of arc characterization for a selected horizontal and nozzle constricted arrangement in blown and unblown conditions, a passive oscillation breaker was designed and successfully tested.

In order to use this slow technology due to the mechanical contact separation time required and because these contacts could be pre-opened before fault triggering, it was necessary to find a way to selectively activate/disable the excitation of the resonance to avoid extinction of the nominal current in the breaker. This requirement was studied in different configurations in a horizontal nozzle constricted setup, where

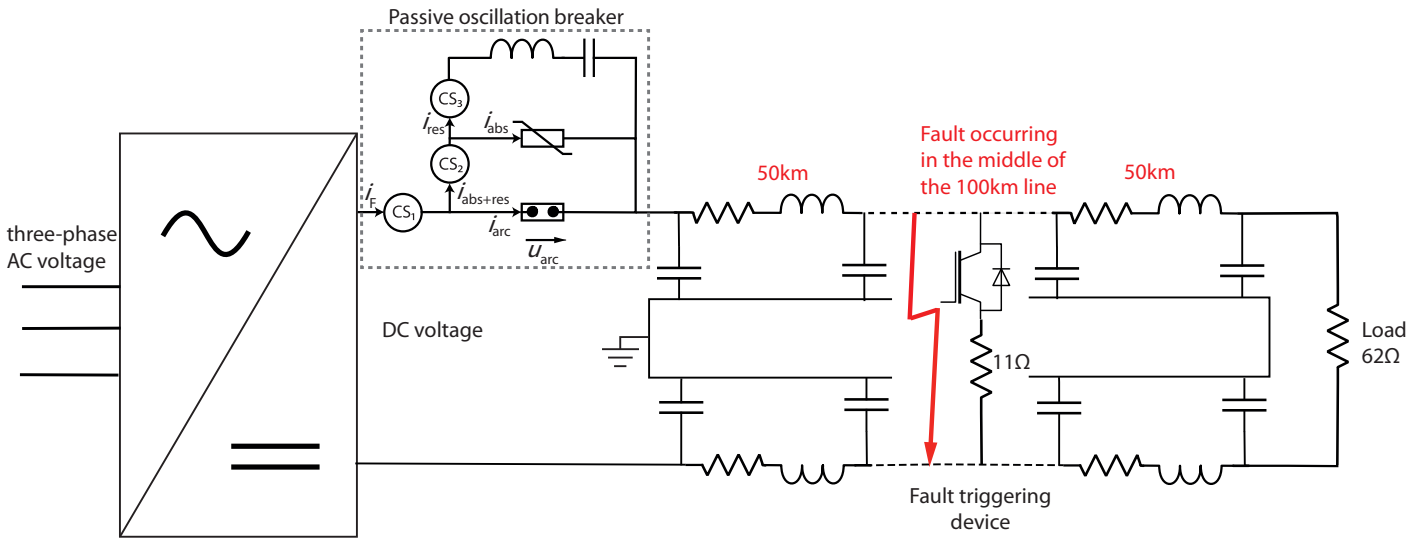

Fig. 22. Breaker-network interaction in the case of a middle line fault (50 km-50 km)

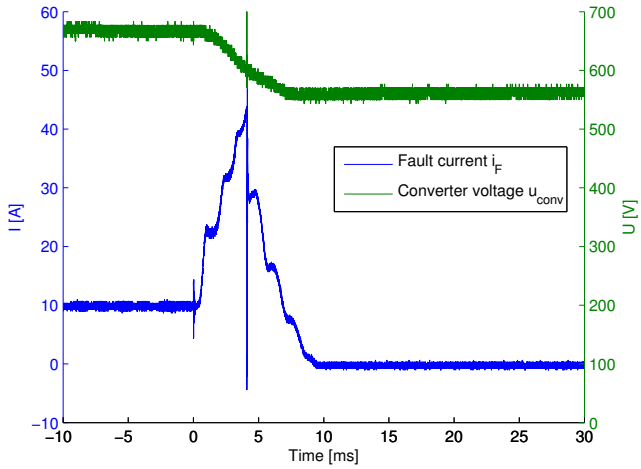

Fig. 23. Fault current i_F and converter voltage u_{conv} profiles

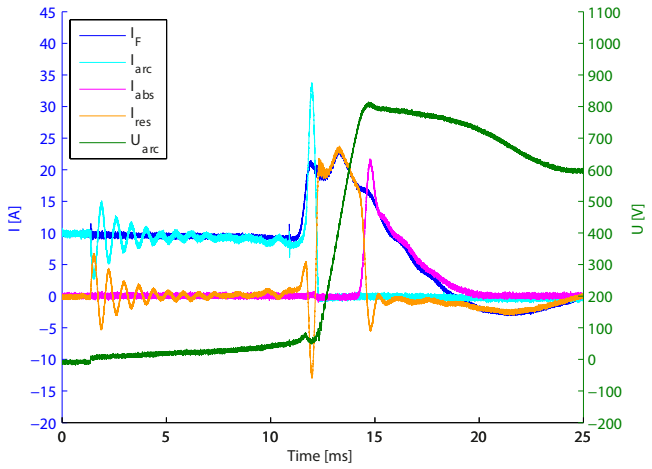

Fig. 24. Middle line (50 km-50 km) fault clearance shot

arc characteristics were derived. These characteristics were inserted in a model to simulate the breaker operation, leading to an optimal design of the resonant path. After its construction, several strategies leading to current extinction were assessed, using an arbitrary current source as feeder. Finally, the breaker was successfully tested in a VSC network.

The modelling of the ablation phenomenon is a further application as well as a research proposal. This work has shown that passive resonance was excited even in the absence of any blow. The assumption on the origin of this effect is the ablation phenomenon, resulting from the interaction of the arc with its surrounding wall. Ablation could be of high interest to design an optimal nozzle shape, in order to have a faster resonance excitation. This could probably be achieved by leaving phenomenological models of arc characterization for CFD models, which can give a better understanding of the physical processes involved in switching arcs. In parallel to these simulations, supplementary measurements of the arc cross-section and length, the arc temperature as well as the ablated mass from the nozzle would be required.

REFERENCES

[1] A. Greenwood, K. Kanngiessner, V. Lesclae, T. Margaard, and W. Schultz, "Circuit breakers for meshed multiterminal HVDC systems Part

I: Introduction DC side substation switching under normal and fault conditions," *Electra*, no. 163, pp. 98-122, Dec. 1995.

[2] A. Greenwood, K. Kanngiessner, V. Lesclae, T. Margaard, and W. Schultz, "Circuit breakers for meshed multiterminal HVDC systems. Part II: Switching of transmission lines in meshed MTDC systems," *Electra*, no. 164, pp. 62-82, Feb. 1996.

[3] L. Bergstrom, L.-E. Juhlin, G. Liss, and S. Svensson, "Simulator Study of Multiterminal HVDC System Performance," *IEEE Trans. Power App. Syst.*, vol. PAS-97, pp. 2057-2066, Nov. 1978.

[4] K. Kanngiesser, H. Ring, and T. Wess, "Simulator study on line fault clearing by DC circuit breakers in a meshed MTDC system," in *International Conf. on AC and DC Power Transmission*, pp. 102-107, London, UK, Sept. 1991.

[5] C. M. Franck, "HVDC Circuit Breakers: A Review Identifying Future Research Needs," *IEEE Transactions on Power Del.*, Vol. 26, No. 2, pp. 998-1007, Apr. 2011.

[6] M. Callavik, A. Blomberg, J. Häfner and B. Jacobson, "The Hybrid HVDC Breaker," *ABB Grid Systems technical paper*, Nov 2012.

[7] W. Grieshaber, J. P. Dupraz, D. L. Penache and L. Violleau, "Development and test of a 120 kV direct current circuit breaker," *Proc. Cigré Session, Paris, France*, 2014.

[8] T. Eriksson, M. Backman and S. Halén, "A low loss mechanical HVDC breaker for HVDC grid applications," *Proc. Cigré Session, Paris, France*, 2014.

[9] V. Billon, J. Taisne, V. Arcidiacono, and F. Mazzoldi, "The Corsican tapping: from design to commissioning tests of the third terminal of the Sardinia-Corsica-Italy HVDC," *IEEE Trans. Power Del.*, vol. 4, pp. 794-799, Jan. 1989.

[10] D. McCallum, G. Moreau, J. Primeau, M. Bahrman, B. Ekehov, and D. Soulier, "Multiterminal integration of the Nicolet Converter Station into the Quebec-New England Phase II HVDC transmission system," in *Proc. of CIGRE 35th Int. Conf. on Large High Voltage Electric Systems*, no. vol.1, pp. 14-103/1-9, Paris, France, Aug.-Sept. 1994.

[11] G. Bathurst and P. Bordignan, "Delivery of the Nan'ao multi-terminal VSC-HVDC system," in *AC and DC Power Transmission, 11th IET International Conference on*, Feb. 2015.

[12] G. Tang, Z. He, H. Pang, X. Huang and X. p. Zhang, "Basic topology and key devices of the five-terminal DC grid," in *CSEE Journal of Power and Energy Systems*, vol. 1, no. 2, pp. 22-35, June 2015.

[13] "NR to Provide Fast Fault Recovery System to Zhoushan 5-Terminal VSC-HVDC," [online], http://www.nrec.com/en/news-content-379.html, Accessed: 03-07-2016, Published: 13-06-2016.

[14] CIGRE JWG A3/B4.34, "Technical requirements and specifications of state-of-the-art DC switching equipment," *CIGRE Technical Brochure*, Unpublished.

[15] M. M. Walter, "Switching arcs in passive resonance HVDC circuit breakers," Ph.D. dissertation ETH Zurich, 2013. http://dx.doi.org/10.3929/ethz-a-010112102

[16] M. K. Bucher, M. M. Walter, M. D. Pfeiffer, and C. M. Franck, "Options for ground fault clearance in HVDC offshore networks," in *IEEE Energy Conversion Congress & Exposition*, Raleigh, North Carolina, USA, 15-20 Sept. 2012.

[17] G. Chaffey and T. C. Green, "Reduced DC circuit breaker requirement on mixed converter HVDC networks," in *PowerTech, 2015 IEEE Eindhoven*.

[18] M. M. Walter and C. M. Franck, "Influence of arc chamber parameters on passive resonance circuit of HVDC circuit breakers," in *CIGRE International Symposium: The Electric Power System of the Future*, Bologna, Italy, 13-15 Sept. 2011.

[19] O. Mayr, "Beiträge zur Theorie des statischen und des dynamischen Lichtbogens," *Arch. f. El.-Tech.*, vd. 37, pp. 588, Germany, Dec. 1943.

[20] M. M. Walter C. M. Franck, "Improved method for direct black-box arc parameter determination and model validation," *IEEE Transactions on Power Del.*, Vol. 29, No. 2, pp. 580-588, Apr. 2014.

[21] M. M. Walter and C. M. Franck, "Optimal Test Current Shape for Accurate Arc Characteristic Determination," *IEEE Transactions on Power Del.*, Vol. 29, Issue 4, pp. 1798-1805, Aug. 2014.

[22] J. Schwarz, "Berechnung von Schaltvorgängen mit einer zweifach modifizierten Mayr-Gleichung", *Elektrotechnische Zeitschrift (ETZ-A)*, bd. 93, pp. 386, Germany, 1972.

[23] G. Pietsch, H. Rijanto and H. G. Thiel, "Schaltlichtbögen im elektrischen Netz," *Elektrotechnische Zeitschrift (ETZ-A)*, vol. 96, pp. 222-226, Germany, 1975.

[24] M. M. Walter and C. M. Franck, "Flexible Pulsed DC-Source for investigations of HVDC circuit breaker arc resistance," in *Proc. of the Int. Conf. on Gas Discharges and their Applications*, pp. 170, Greifswald Germany, 2010.

[25] H. Rijanto, "Ein experimentelles Verfahren zur Bestimmung von Lichtbogenkenngrössen - Stromüberlagerungsverfahren," Dissertation, TU Hannover, 1975.

Julien Thomas received his BSc in electrical engineering from EPFL, Switzerland in 2012 and his MSc in energy science and technology from ETH Zurich, Switzerland in 2014. During his master's degree thesis, he worked on the design and the construction of a small scale HVDC circuit breaker. Currently, he is working for ABB Switzerland Ltd, as control system engineer for substation automation.

Geraint Chaffey received the M.Eng. degree in electrical and electronic engineering from Cardiff University, U.K., in 2012 and the Ph.D. degree from Imperial College London, U.K., in 2017. His doctoral thesis was titled 'The Impact of Fault Blocking Converters on HVDC Protection'. He is presently a postdoctoral researcher at Imperial College London, where his main research interests are focused on HVDC converter topology, HVDC circuit breakers and HVDC protection systems.

Christian M. Franck (M04, SM11) received the diploma in physics from the University of Kiel, Kiel, Germany in 1999 and the Ph.D. degree in physics from the University of Greifswald, Greifswald, Germany in 2003. He was Scientist and Group Leader for gas circuit breakers and high-voltage systems with the Swiss corporate research center of ABB, Dttwil, Switzerland, from 2003 to 2009. Currently, he is Associate Professor for High Voltage Technology at ETH Zurich, Zurich, Switzerland.